Supplementary Materials

Antibiotics as a selective driver for conjugation dynamics

Allison J. Lopatkin[1], Shuqiang Huang[1], Robert P. Smith[3], Jaydeep K. Srimani[1], Tatyana Sysoeva[1], Sharon Bewick[4], David Karig[5], and Lingchong You[1, 2,+]

[1]Department of Biomedical Engineering, Duke University, Durham, North Carolina, USA.

[2]Center for Genomic and Computational Biology, Duke University, Durham, North Carolina, USA.

[3]Department of Biological Sciences, Halmos College of Natural Sciences and Oceanography, Nova Southeastern University, Fort Lauderdale FL, USA.

[4]Department of Biology, University of Maryland, College Park, MD 20742, USA

[5]Johns Hopkins University Applied Physics Laboratory, Laurel, MD, USA

[+] Correspondence and requests for materials should be addressed to Lingchong You. E-mail: you@duke.edu; Tel: 919-660-8408; Fax: 919-668-0795.

This file includes:

Other Supplementary material for this manuscript include:

Videos S1 to S2

Model development

The full kinetic model consisting of three ordinary differential equations (ODE) accounts for antibiotic-modulated growth dynamics of each population, as well as the conjugation between the donor (*G*) and recipient cells (*R*) to generate transconjugants (*Y*). The model has five parameters: the carrying capacity (N_m), the growth rates of each population (μ_R, μ_G and μ_Y), and the conjugation efficiency (η_C). We estimated each parameter experimentally. In particular, we based growth rates on R^-, G^+, and Y plate reader dose response quantification from high-temporal resolution growth curves (Fig. S4a). For populations that were sensitive to the tested antibiotic (e.g. R^- with Kan and G^+ with Cm), growth rates were estimated by fitting to a Hill equation (Eq. 4, Table S4a). For those that were resistant to the antibiotic (e.g. R^- with Cm, R^k with Kan, G^+ with Kan, G^+ with Kan + 4 μg/mL Cm, Y with Cm, and Y with Kan), growth rates were fit to a linear line, $\mu = \mu_{max} - mA$, where m is a constant and μ_{max} is the growth rate in the absence of the antibiotic. Since the term mA is always much smaller than μ_{max} (Table S4a), we assumed a constant growth rate approximately equal to μ_{max} for modeling analysis (Table S4b). Lastly, we estimated η_C as the maximum upper limit obtained experimentally (1×10^{-11}). The qualitative trends from model predictions remain the same when η_C is varied, unless it is too large (Fig. S4b).

$$\frac{dG}{dt} = \mu_G G\left(1 - \frac{R+G+Y}{N_m}\right), \quad \text{S1}$$

$$\frac{dR}{dt} = \mu_R R\left(1 - \frac{R+G+Y}{N_m}\right) - \eta_C R(G+Y), \quad \text{S2}$$

$$\frac{dY}{dt} = \mu_Y Y\left(1 - \frac{R+G+Y}{N_m}\right) + \eta_C R(G+Y). \quad \text{S3}$$

In our experiments, μ_G and μ_R depend on the antibiotic doses; μ_Y is largely independent of the antibiotic dose (Table S4a), or $\mu_Y \approx \mu_{Y_{max}}$= constant.

We further non-dimensionalized the equations to facilitate modeling analysis, which gives our full, dimensionless model:

$$\frac{dg}{d\tau} = \mu_g g(1 - r - g - y), \quad \text{S4}$$

$$\frac{dr}{d\tau} = \mu_r r(1 - r - g - y) - \eta'_C r(g+y), \quad \text{S5}$$

$$\frac{dy}{d\tau} = y(1 - r - g - y) + \eta'_C r(g+y), \quad \text{S6}$$

where $g = \frac{G}{N_m}$, $r = \frac{R}{N_m}$, $y = \frac{Y}{N_m}$, $a = \frac{A}{K_R}$, $\tau = t\mu_{Y_{max}}$, $\mu_g = \frac{\mu_G}{\mu_{Ymax}}$, $\mu_r = \frac{\mu_R}{\mu_{Ymax}}$, and $\mu_y = \frac{\mu_Y}{\mu_{Ymax}} = 1$, and $\eta'_C = \frac{\eta_C N_m}{\mu_{Ymax}}$ (See Table S4c for a full list of dimensionless parameters and values).

Assuming $y << g$ at an early enough time, our simplified model can be written as:

$$\frac{dg}{d\tau} = \mu_g g(1 - r - g - y), \quad \text{S7}$$

$$\frac{dr}{d\tau} = \mu_r r(1 - r - g - y) - \eta'_C rg, \quad \text{S8}$$

$$\frac{dy}{d\tau} = y(1 - r - g - y) + \eta'_C rg, \quad \text{S9}$$

This assumption can be relaxed, and our full model predicts the same outcomes (Fig. S4c).

Buffer population

The model can be extended to account for a buffer population *(b)*. Upon accepting a mobile plasmid from *g* or *y*, it turns into the donor *g* and can transfer the mobile plasmid to *r* or *b*:

$$\frac{dg}{d\tau} = \mu_g g(1 - r - g - y - b) + \eta'_C b(g + y), \quad \text{S10}$$

$$\frac{dr}{d\tau} = \mu_r r(1 - r - g - y - b) - \eta'_C r(g + y), \quad \text{S11}$$

$$\frac{dy}{d\tau} = y(1 - r - g - y - b) + \eta'_C r(g + y), \quad \text{S12}$$

$$\frac{db}{d\tau} = \mu_b b(1 - r - g - y - b) - \eta'_C b(g + y), \quad \text{S13}$$

where $\mu_b = \frac{\mu_B}{\mu_{Ymax}}$. Similar to the full model, assuming *y* << *g, b,* we have:

$$\frac{dg}{d\tau} = \mu_g g(1 - r - g - y - b) + \eta'_C gb, \quad \text{S14}$$

$$\frac{dr}{d\tau} = \mu_r r(1 - r - g - y - b) - \eta'_C rg, \quad \text{S15}$$

$$\frac{dy}{d\tau} = y(1 - r - g - y - b) + \eta'_C rg, \quad \text{S16}$$

$$\frac{db}{d\tau} = \mu_b b(1 - r - g - y - b) - \eta'_C gb. \quad \text{S17}$$

This simplification can be relaxed and does not influence the model predictions (Fig. S6c).

Parameter values

All growth rates are based on plate-reader measurements (Fig. S4a) and are normalized with respect to μ_y. For experimental analysis done in the microfluidic device, we used these growth estimates as a guide to choose parameters that captured the four qualitative trends (Fig. 3b top row, Table S4c). The simulations run for 16 arbitrary time units (A.U.) (τ). To capture the power law correlation (Fig. 4a) at different time points, simulations were run from 12 to 16 A.U, with the initial values of *r* and *g* set at 1×10^{-3} (see Table S4). For simulations including a buffer population, the initial density of each population was equal to $\frac{1\times10^{-3}}{3}$.

Modulating population structure (Fig. 4)

To investigate the extent to which antibiotic-mediated changes in population structure influence the overall promotion of f_y, we implemented a stochastic simulation where we drew μ_r and μ_g from a normal distribution with mean 1 and standard deviation 0.3 for 100 iterations, and quantified the percentage of each population for each combination of growth rates. In general, random growth rates represent the unknown influence of antibiotic use. Randomizing the growth rates also expands the possible selection space to include all potential dose responses of the two parents. The power law correlation was examined for a range of $\eta_C$values. In general, the power law relationship holds over 6 orders of magnitude of η_C, but becomes more variable as η_C increases.

Supplemental figures and legends

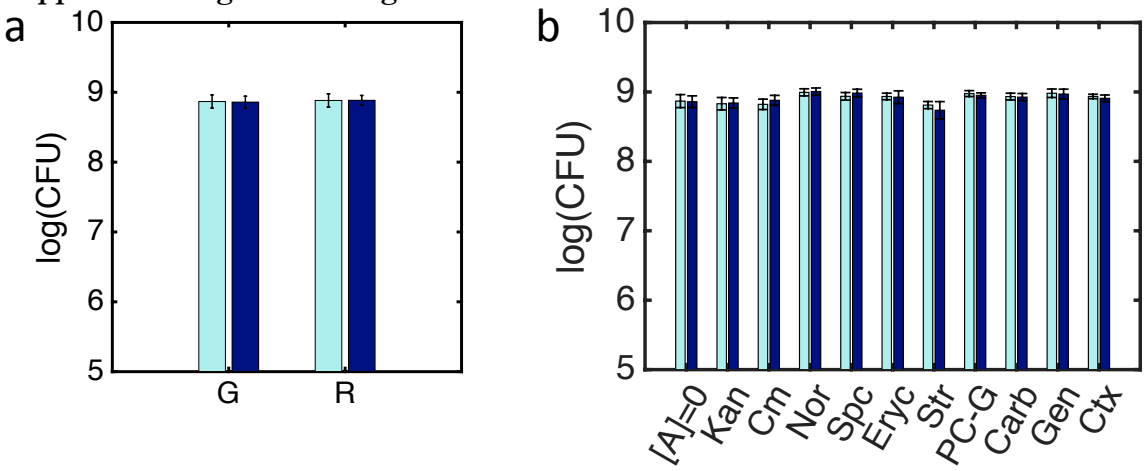

Fig. S1. No significant change in densities of parental populations during 1-hr incubation. Colony forming units (CFU) were counted at time = 0 (light blue) and time = 1 (dark blue) hour of incubation at room temperature in M9 minimal media to ensure both growth (a) and death (b) is negligible ($P > 0.8$, and $P > 0.2$ respectively) over this time period for each antibiotic. Error bars are standard deviations of technical replicates, which are anywhere from four to six per experiment. Antibiotic [A] concentration used was $4 \times IC_{50}$ value (see Table S3).

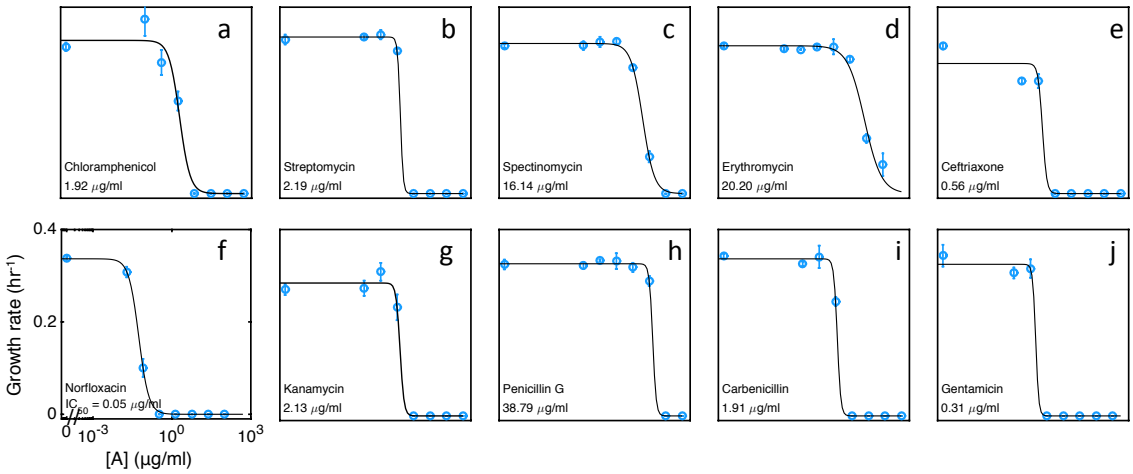

Fig. S2. Quantifying the IC_{50} value of MG1655 for each antibiotic

IC_{50} values (inset) were determined using high-resolution growth curves obtained from plate-reader measurements. Slashes on the x-axis indicate a change from linear to logarithmic scaling. Concentrations of 0, 0.95, 0.399, 1.66, 6.9, 28.8, 120, and 500μg/ml were used for antibiotics Kan, Cm, Carb, Str, Spc, Ctx, and PC-G. Concentrations of 0, 0.019, 0.08, 0.33, 1.38, 5.77, 24.01 and 100 μg/ml were used for Nor and Eryc. Lastly, concentrations 0, 0.047, 0.20, 0.83, 3.46, 14.4, 60.03, and 250 μg/ml were used for Gen. The exponential growth phase was log-transformed and fit to a linear line. Slopes of log-fitted lines are used as growth rates (μ). Error bars represent standard deviations from three technical replicates. Black lines indicate fitted curves based on equation 4 (main text). Antibiotics used are (a) Cm, (b) Str, (c) Spc, (d) Eryc, (e) Ctx, (f) Nor, (g) Kan, (h) PC-G, (i) Carb, and (j) Gen. Cell strain G^+ was used for all growth curve quantifications except for (g), where R^- is used since G^+ is resistant to Kan.

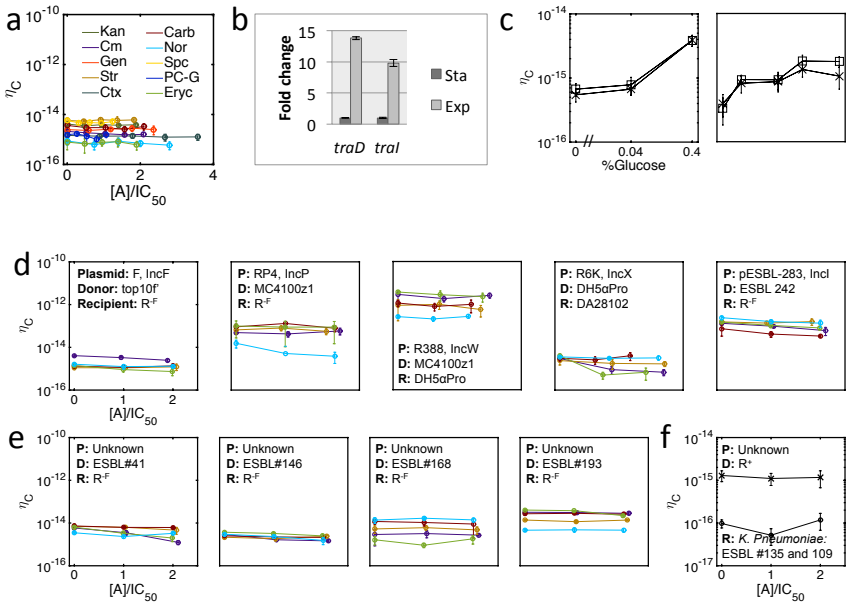

Fig. S3. Modulation of conjugation efficiency

(a) Measured conjugation efficiency values without normalization (same data as Fig. 2b). Day-to-day variations exceed those within a given experiment. Antibiotics used are described in Table S2. Concentrations and IC_{50} values used can be found in Table S3a. Standard deviations are from four-six replicates.

(b) qRT-PCR data for cells harvested from stationary (Sta) and exponential (Exp) phase cultures. The same clone was used for both. RNA was isolated and immediately reverse-transcribed into cDNA. *traD* encodes for coupling protein, and *traI* for relaxase. *ffh* is used as a housekeeping gene; transfer genes are first normalized with respect to *ffh* to account for differences in quantity from Sta and Exp cultures, and then normalized with respect to Sta gene expression to quantify the fold change.

(c) Influence of increasing glucose concentration on conjugation efficiency in the presence of low (2 μg/mL Kan, same as Fig. 2c right panel) or high (right, 4 μg/mL Kan) antibiotic concentration, without normalization of η_C. Boxes and crosses indicate with and without antibiotic, respectively. Glucose significantly increases ($P<0.01$, left-sided one-tailed t-test) the efficiency (7-fold for low and 5-fold for high) regardless of the antibiotic concentration present.

(d) Non-normalized conjugation efficiency of five native self-transmissible conjugative systems F, RP4, R388, R6K, and pESBL-283 for five antibiotics tested (same as Fig. 2d i-v). Colors represent different antibiotics, corresponding to the same colors in (a), namely Eryc (green), Str (gold), Cm (purple), Carb (maroon), and Nor (blue). The plasmid, donor, and recipient used are labeled in each figure. See Table S1 for the complete list of strain and plasmid details. Antibiotic concentrations and statistical testing for each pair are listed in Table S3b.

(e) Non-normalized conjugation efficiency of clinical ESBL-producing donors with unknown conjugation machinery and R^{-F} recipient, for five antibiotics. Colors represent different antibiotics, corresponding to the same colors in (a), namely Eryc (green), Str, (gold), Cm (purple), Carb (maroon), and Nor (blue). Antibiotic concentrations and statistical testing for each pair are listed in Table S3b.

(f) Non-normalized conjugation efficiency for inter-species conjugation between *K. pneumoniae* ESBL-producing clinical isolates and R^{+} donor. Crosses indicate isolate #135, and squares indicate isolate #109. Here, 0, 2, and 4 μg/mL Str are used. Statistical testing for each pair is listed in Table S3b.

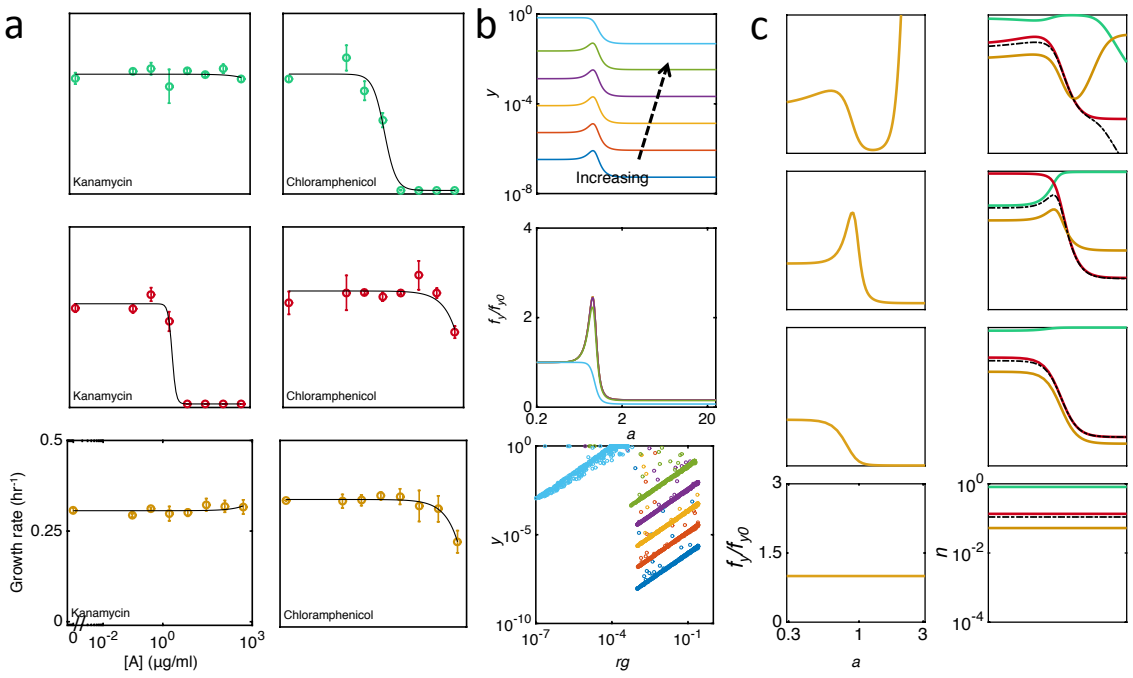

Fig. S4. Population growth quantification

(a) Growth rates were analyzed similarly to quantifying the IC_{50} for all antibiotics (Fig. S2). Antibiotic concentrations were logarithmically varied over three orders of magnitude and the effects of seven concentrations were tested, including zero as control for the 8th point. Slashes on the x-axis indicate a change from linear to logarithmic scale. The same concentrations as in Fig. S2 were used. The exponential phase of each growth curve captured over the time span of 12 hours was log-transformed and fit to a linear line. The slope of the fitted line gives the growth rate. Error bars represent standard deviations from three replicates. Top row: G^+ cells were used to determine growth rates for treatment with Kan and Cm. Middle row: R^- cells were used to determine growth rates for treatment with Kan and Cm. Bottom row: Pre-conjugated Y cells were used to determine growth rates for treatment with Kan and Cm.

(b) Choosing η_C parameter as an average of all CFU experiments. Maximum estimated η_C value is used, 1×10^{-11}. Example using growth dynamics from Fig. 3b iii is shown. η_C' is varied 6 orders of magnitude to determine its influence on the fraction of transconjugant dynamics. Top panel: Green line represents results from the base value. Any efficiency below this results in qualitatively similar trends, while increasing higher (light blue) can lose the biphasic dependence. Middle panel: All curves collapse onto the same line when normalized to the fraction in the absence of antibiotics (f_{y_0}), unless the conjugation efficiency is higher than the base value. Bottom: The same values of η_C' are used, and the influence on the power law correlation is examined.

(c) Modeling results using the full, non-simplified kinetic model (Eq. S4-S6). Left panel is the fraction of transconjugants (f_y) normalized to the fraction in the absence of antibiotics (f_{y_0}), and right panel shows the density of each of the three populations *r*, *g*, and *y*. Black dotted line indicates *rg*. Qualitative trends remain the same as with simplified version (Fig. 3b), demonstrating that the simplifications can be relaxed.

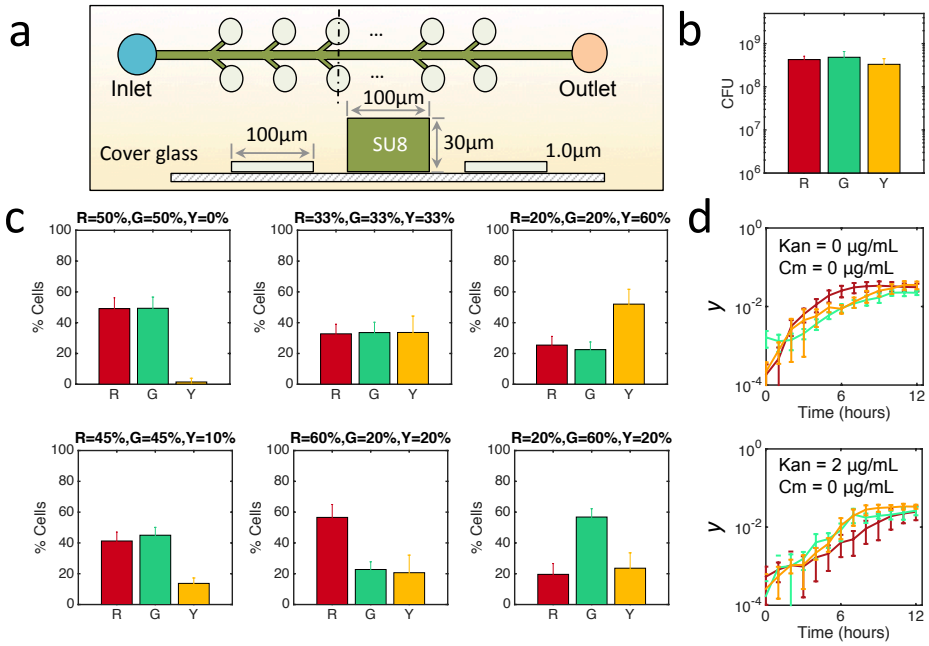

Fig. S5. Microfluidic platform and image calibration

(a) Microfluidic schematic. Each chip contains 6 channels with 24 trapping chambers. Cells and media were loaded through the main channel. The main channel is 100 μ m in width and 30 μ m in height. Trapping chambers are 100 μ m in diameter, and ~1.3 μ m in height. Each trapping chamber has a neck of the same height as the main channel to facilitate cell loading. 10 chamber positions were selected for monitoring.

(b) R^-, G^+ and Y strains were calibrated by plating after an initial 2-hour sub-culture, typical for each microfluidic experiment. Analysis shows no significant difference in R^-, G^+, or Y densities (measured as CFU).

(c) R^-, G^+ and Y were mixed in pre-defined ratios, shown at the top of each bar plot. Volume was used as a proxy for cell density since CFU counts showed no significant difference between the three populations (Fig. S5b). Measured fluorescence values detected by colocalization and thresholding algorithms are shown as bar plots, and error bars are standard deviations of an average of 10 replicates. Each plot shows different mixed ratios to ensure computational accuracy.

(d) Reproducibility in the microfluidic chip. X-axis is time in hours, and y-axis ($y = \frac{Y}{N_m}$) is total Y pixels normalized by carrying capacity of pixels in the chamber (=6×10^5 pixels/chamber). Error bars are shown for once every hour, up to the 12th hour of 8-10 chamber replicates. Each color represents an experiment done on a different day. y is statistically the same for all three days at the 12th hour. Top panel shows Kan and Cm = 0 μ g/mL, and the bottom panel shows Kan = 2 μ g/mL and Cm = 0 μ g/mL.

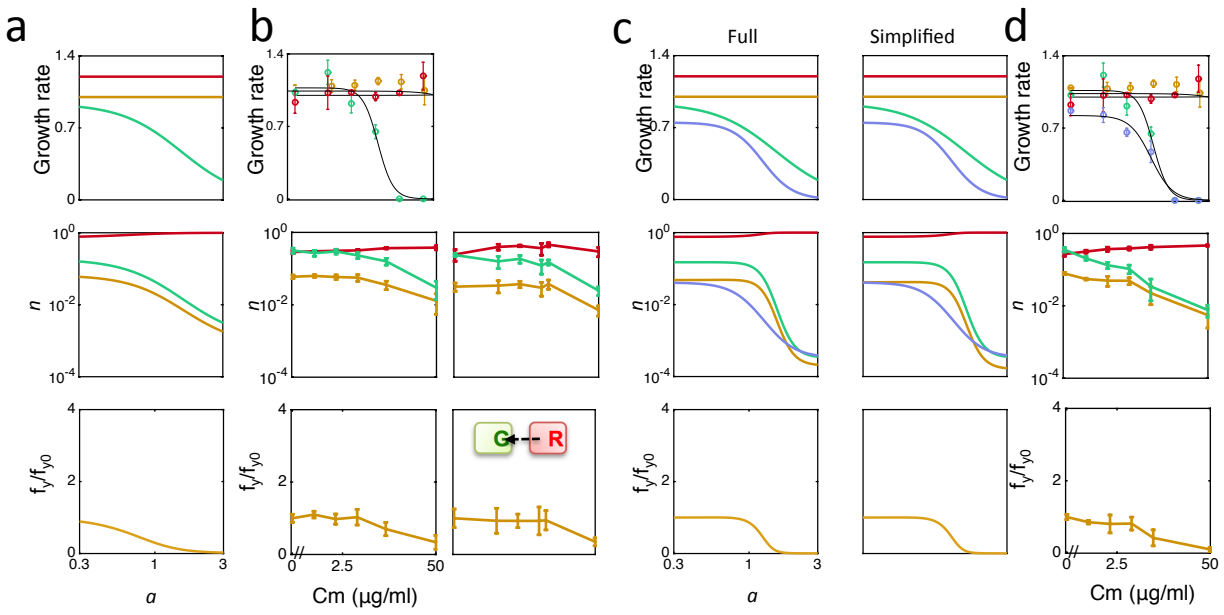

Fig. S6 Generality of antibiotic selection on conjugation dynamics

(a) Using the full model, Cm is varied instead of Kan. In this scenario, *r* is resistant to the antibiotic while *g* is sensitive. This scenario is the reverse of that described in Fig. 3b ii. The full model predicts that transconjugant dynamics are maintained as long as the growth rate trends are maintained. Top row: growth rates of each population. Middle row: density (*n*) of each population. Bottom row: the fraction of *y*, f_y, normalized to the fraction in the absence of antibiotic, f_{y_0}.

(b) **Left:** Microfluidic data confirmed modeling predictions. Increasing Cm concentration did not influence f_y dynamics as long as the growth trends were maintained (top row). Middle row: the density of each population normalized by the chamber carrying capacity (N_m = 6×10^5 pixels/chamber). Bottom row: f_y normalized to the fraction in the absence of antibiotic, f_{y_0}.

Right: f_y dynamics are independent of the direction of transfer. We switched *oriT* sequence such that R transfers a copy of its plasmid to G, and used Cm to test how the dynamics change (R$^+$ and G$^-$ in Table S1). Top row: same as that on the left, as the growth rates have not changed. Middle row: the density of each population normalized to N_m. Bottom row: f_y normalized to the fraction in the absence of antibiotic, f_{y_0}.

(c) The full model predicts that the presence of a buffer population (*b*) has negligible influence on f_y dynamics. Simulation conditions are the same as described in Fig. 3b. Top row: the growth rates of each population, where the buffer population is in purple. Middle row: the density of all four populations. Bottom row: normalized f_y, taking into account only the parents (i.e.. $f_y = \frac{y}{r+g+y}$). Left column is the full model (Eq. S10-13), and right column is the simplified model (Eq. S14-17).

(d) Experimental data supports modeling predictions that the buffer population (*b*) has negligible influence on the conjugation dynamics. The growth rates of all four populations are shown in the top row. *b* carries no fluorescence, and so the total density could not be computed. As f_y does not take into account the buffer population, this has no influence on quantification in the bottom row.

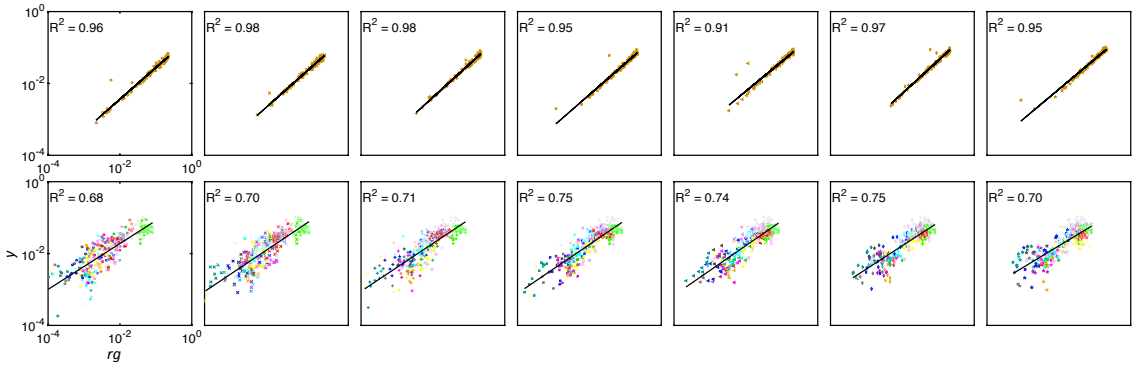

Fig. S7 Power law correlation for individual time points

(a) Modeling results from Fig. 4a separated into individual plots for each time point. Stochastic simulation with randomized parameters μ_r and μ_g, and collecting *r g* and *y*. Parameters are randomly generated from a normal distribution with mean of 1 and standard deviation of 0.3, and collected for 7 time points spanning between 12 and 16 A.U., from left to right. X-axis is *rg* and y-axis is *y*. Different markers indicate different time points (o, x, +, square, <, diamond, and *). The power law was fit to a linear regression where $log(y) = b_1 log(rg) + b_0$, where b_1= 0.83, 0.93, 0.90, 0.92, 0.93, 0.91, and 0.92, and b_0= -1.67, -1.38, -1.32, -1.20, -1.09, -1.05, and -0.091 from left to right respectively. $P<1\times10^{-4}$ (linear regression) for all time points.

(b) Experimental results from Fig. 4b separated into individual plots for each time point. Here, *r*, *g*, and *y* are measured by normalizing the respective pixel number for each (mCherry, GFP, and the colocolization of the two colors), normalized by the carrying capacity of pixels in the chamber ($=6\text{x}10^5$ pixels/chamber). Data used from seven experiments. From left to right, each plot shows result from the 6th to the 12th hour; colors indicate independent experiments, and shading indicates varied antibiotic concentration within each experiment (lightest [A] = 0 to darkest, see Table S5a for color designation). Different markers indicate different time points, from 6th to 12th hour (o, x, +, square, <, diamond, and *). The power law was fit to a linear regression where $log(y) = b_1 log(rg) + b_0$, where b_1= 0.64, 0.67, 0.67, 0.68, 0.69, 0.65, and 0.60, and b_0= -1.03, -0.88, -0.89, -0.90, -0.91, -1.11, and -1.34 from left to right respectively. $P<1\times10^{-4}$ (linear regression) for all time points.

Supplemental tables

Table S1. Strains and plasmids used in this study

A combined list of all strains and plasmids used in this study with a description of each.

Name	Strain and Genotype	Description of strain and experimental use	Resistance
R⁻	*E. coli* MG1655 (K-12 F⁻ λ⁻ *ilvG⁻ rfb-50 rph-1* / pTetmCherry p15A *cm*ᴿ FHR *oriT*ᵐ *tet*ᴿ)	Strain containing Tet-inducible copy of mCherry and the FHR helper plasmid. This strain was used as a recipient (Fig. 2b, 3Dii-iv, and S6d).	Cm, Tet
Rᵏ	*E. coli* MG1655 (K-12 F⁻ λ⁻ *ilvG⁻ rfb-50 rph-1* / pTetmCherry p15A *kan*ᴿ FHR *oriT*ᵐ *tet*ᴿ)	Strain containing Tet-inducible copy of mCherry with *kan*ᴿ instead of *cm*ᴿ and the FHR helper plasmid This strain was used as a recipient (Fig. 3d i).	Kan, Tet
R⁺	*E. coli* MG1655 (K-12 F⁻ λ⁻ *ilvG⁻ rfb-50 rph-1* / pTetmCherry *oriT* p15A *cm*ᴿ FHR *oriT*ᵐ *tet*ᴿ)	Strain containing a transferable Tet-inducible copy of mCherry and the FHR helper plasmid. This strain was used as a donor strain (Fig. S3f and S6b).	Cm, Tet
R⁻ᶠ	*E. coli* MG1655 (K-12 F⁻ λ⁻ *ilvG⁻ rfb-50 rph-1* / pTetmCherry p15A *cm*ᴿ)	Strain containing Tet-inducible copy of mCherry and no helper plasmid. This was used as recipient for generality experiments (Fig. 2c, and those designated in Fig. 2d).	Cm
G⁺	*E. coli* MG1655 (K-12 F⁻ λ⁻ *ilvG⁻ rfb-50 rph-1* / pUA66ᵀ *oriT* SC101 *kan*ᴿ FHR *oriT*ᵐ *tet*ᴿ)	Strain containing a transferrable IPTG-inducible copy of GFP with *oriT* and the FHR helper plasmid. This strain was used as a donor (Fig. 2b-c, Fig. 3d, Fig. S6d).	Kan, Tet
G⁻	*E. coli* MG1655 (K-12 F⁻ λ⁻ *ilvG⁻ rfb-50 rph-1* / pUA66 SC101 *kan*ᴿ FHR *oriT*ᵐ *tet*ᴿ)	Strain containing IPTG-inducible copy of GFP without *oriT* and the FHR helper plasmid. This strain was used as a recipient (Fig. S6b). It was also used as control for *oriT* specificity (Fig. 3c and Video S2).	Kan, Tet
B	*E. coli* MG1655 (K-12 F⁻ λ⁻ *ilvG⁻ rfb-50 rph-1* / FHR *oriT*ᵐ *tet*ᴿ)	Strain containing only the FHR helper plasmid. This strain was used as the buffer (Fig. S6d).	Tet
F donor	*E. coli* TOP10F' (F´{*lac*Iᵠ, Tn*10*(Tetᴿ)} *mcr*A Δ(*mrr-hsd*RMS-*mcr*BC) Φ80*lacZ*ΔM15 Δ*lac*X74 *rec*A1 *ara*D139 Δ(*ara leu*) 7697 *gal*U *gal*K *rps*L (Strᴿ) *end*A1 *nup*G)	Strain containing native, self-transferrable F plasmid (Fig. 2d i).	Str, Tet
RP4 donor	*E. coli* MC4100z1 (F⁻ *araD139 Δ(argF-lac)U169 rpsL150* (Strᴿ)*relA1 flbB5301 deoC1 ptsF25 rbs*R / RP4 IncPα Tra+*amp*ᴿ *kan*ᴿ *tet*ᴿ)	Strain containing the native RP4 self-transmissible plasmid. This strain was used as a donor (Fig. 2d ii).	Kan, Amp, Str
R388 donor	*E. coli* MC4100z1 (F⁻ *araD139 Δ(argF-lac)U169 rpsL150* (Strᴿ)*relA1 flbB5301 deoC1 ptsF25 rbs*R / R388 IncW Tra+*str*ᴿ *spc*ᴿ *sul*ᴿ *tm*ᴿ)	Strain containing the native R388 self-transmissible plasmid. This strain was used as a donor (Fig. 2d iii).	Str, Spc Sul, Tm
R388 recipient	*E. coli* DH5α*Pro:GFP kan*ᴿ (F⁻ *endA1 glnV44 thi-1 recA1 relA1 gyrA96 deo*R *nupG purB20* φ80d*lacZ*ΔM15 Δ(*lacZYA-argF*)U169, hsdR17(*rK⁻mK⁺*), λ⁻)	Strain with a gene conferring Kan resistance and GFP integrated into the chromosome. This strain was used as a recipient (Fig. 2d iii).	Kan, Strep
R6K donor	*E. coli* DH5α*Pro:GFP* kanᴿ (F⁻ *endA1 glnV44 thi-1 recA1 relA1 gyrA96 deo*R *nupG purB20* φ80d*lacZ*ΔM15 Δ(*lacZYA-argF::gfp (kan*ᴿ*)*)U169, hsdR17(*rK⁻mK⁺*), λ⁻ / R6K *IncX kan*ᴿ *ery*ᴿ *amp*ᴿ)	Strain containing the native R6K self-transmissible plasmid, with a gene conferring Kan resistance and GFP integrated into the chromosome. This strain was used as a donor (Fig. 2d iv).	Eryc, Kan, Amp

R6K recipient	*E. coli* DA28102 (K-12 F⁻ λ⁻ *ilvG⁻ rfb-50 rph-1 galK*::*cat*-J23101-mTagBFP2)[1]	Strain created by Gullberg *et al*,[1] containing no plasmid, with a gene conferring Cm resistance integrated into the chromosome and BFP. This strain was used as a recipient (Fig. 2d iv).	Cm
ESBL242 donor	*E. coli* isolate carrying the IncI pESBL-283 plasmid isolated from chicken meat.	Strain obtained from and characterized by Händel et al. originally isolated from chicken meat by B Wit of the Netherlands Food and Consumer Product Safety Authority[2] (Fig. 2d v).	CTX-M1, Amp
ESBL donor	Four *E. coli* Isolates: Numbers 41, 146, 168 and 193 ($pbla_{CTX}$ cro^{R}	Clinical *E. coli* isolate of unknown genotype containing a conjugative plasmid that confers resistance to ESBLs. Isolation occurred as described in Supplementary Methods. Full plasmid sequence unknown (Fig. 2d vi-ix).	Extended spectrum β - lactams (including Ctx)
ESBL recipient	Two ESBL *Klebsiella pneumonia* isolates: Numbers 109 and 135 ($pbla_{CTX}$ ctx^{R})	A clinical *K. pneumonia* isolate of unknown genotype containing resistance to ESBLs, but are incapable of acting as donors to *E. coli* recipients and are thus used as donors (Fig. S3f).	Extended spectrum β - lactams (including Ctx)

Table S2. Antibiotics used in this study

Full list of antibiotics used to test the effect on conjugation efficiency are described here, including their class, mode of action, and purchasing information.

Antibiotic	Class	Description	Vendor/catalog number
1. Kanamycin (Kan)	Aminoglycoside	Inhibits protein synthesis binding to 30S ribosomal subunit	Omnipur #5880
2. Gentamicin (Gen)	Aminoglycoside	Inhibits protein synthesis binding to 30S ribosomal subunit	Gibco #1575-060
3. Streptomycin (Str)	Aminoglycoside	Inhibits protein synthesis binding to 30S ribosomal subunit	Sigma Aldrich #S6501
4. Spectinomycin (Spc)	Aminoglycoside	Inhibits protein synthesis binding to 30S ribosomal subunit	MP Biomedicals #158993
5. Penicillin G (PC-G)	β -lactam	Inhibits peptidoglycan cross-links in the bacterial cell wall	Sigma Aldrich #P7794
6. Carbenicillin (Carb)	β -lactam	Inhibits peptidoglycan cross-links in the bacterial cell wall	Molecular Biological International #MBPC2202
7. Ceftriaxone (Ctx)	β -lactam (Cephalosporin 3rd generation)	Inhibits peptidoglycan cross-links in the bacterial cell wall	Sigma Aldrich #C7039
8. Erythromycin (Eryc)	Macrolide	Reversible binding on 50S ribosomal subunit inhibiting protein synthesis	Sigma Aldrich #E5389
9. Chloramphenicol (Cm)	Amphenicol	Prevents protein chain elongation by inhibiting peptidyl transferase activity of the ribosome	Fisher Scientific BP904-100
10. Norfloxacin (Nor)	Quinolone	Inhibits enzymes necessary for bacterial DNA replication	Sigma Aldrich # N9890

Table S3. Effects of antibiotic on conjugation efficiency

One-sided left-tailed t-test was used to test whether any conjugation efficiency in the presence of antibiotics, $\eta_C(A_i)$, was significantly greater than the conjugation efficiency in the absence of antibiotic, η_{C0}, where i is the index of antibiotic concentration tested. Each concentration was compared against η_{C0}, and the P-values are shown. There was no statistically significant increase (P>0.15, one-sided left-tailed t-test) for all antibiotics and concentrations tested. All donor and recipient combinations are shown in individual sub-tables. IC_{50} values and concentrations used for each experiment are included.

(a) Data corresponding to Fig. 2b for plasmid F_{HR}. IC_{50} values here are for MG1655.

Antibiotic	**IC_{50} (μ g/mL) and corresponding strain**	**Concentration used (μ g/mL)**	$\eta_{C0}:\eta_C(A_1)$	$\eta_{C0}:\eta_C(A_2)$	$\eta_{C0}:\eta_C(A_3)$	$\eta_{C0}:\eta_C(A_4)$
Kan	2.13	0, 1, 2, 3, 4	0.88	0.71	0.84	0.70
Gen	0.31	0, 0.183, 0.367, 0.55, 0.733	0.68	0.29	0.16	0.50
Str	2.19	0, 1, 2, 3, 4	0.72	0.29	0.48	0.34
Spc	16.14	0, 5, 10, 15, 20	0.95	0.90	0.97	0.76
PC-G	38.79	0, 10.4, 20.7, 31.1, 41.5	0.29	0.72	0.99	0.58
Carb	1.91	0, 1, 2, 3, 4	0.79	0.81	0.92	0.67
Ctx	0.56	0, 0.5, 1, 1.5, 2	0.64	0.60	0.76	0.73
Eryth	20.20	0, 9.6, 19.2, 28, 38.4	0.69	0.53	0.45	0.82
Cm	1.92	0, 1, 2, 3, 4	0.96	0.99	1.00	0.99
Nor	0.05	0, 0.037, 0.07, 0.1, 0.14	0.94	0.55	0.88	0.96

(b) Data corresponding to Fig. 2d and Fig. S3d-f. For each pair, IC_{50} values of the recipient was used to determine antibiotic concentrations, unless the recipient was resistant to the tested antibiotic or the concentrations were lethal to the other strain. In these cases, the donor IC_{50} was used. MG1655 IC_{50} values for all ESBL conjugation experiments were used.

Plasmid: F

Antibiotic	**IC_{50} (μ g/mL)**	**Concentration used (μ g/mL)**	$\eta_{C0}:\eta_C(A_1)$	$\eta_{C0}:\eta_C(A_2)$
Str	2.19 (R^F)	0, 2, 4	0.53	0.32
Carb	1.9 (R^F)	0, 2, 4	0.82	0.43
Eryth	20.20 (R^F)	0, 19.2, 38.4	1.00	1.00
Cm	0.7 (F donor)	0, 0.7, 1.4	0.97	1.00
Nor	0.05 (R^F)	0, 0.05, 0.1	0.83	0.91

Plasmid: RP4

Antibiotic	IC_{50} (μ g/mL)	Concentration used (μ g/mL)	$\eta_{C0}:\eta_C(A_1)$	$\eta_{C0}:\eta_C(A_2)$
Str	2.19 (R^F)	0, 2, 4	0.16	0.78
Carb	1.9 (R^F)	0, 2, 4	0.06	0.72
Eryth	20.20 (R^F)	0, 19.2, 38.4	0.58	0.58
Cm	0.7 (RP4 donor)	0, 0.7, 1.4	0.82	0.18
Nor	0.05 (R^F)	0, 0.05, 0.1	0.83	0.91

Plasmid: R388

Antibiotic	IC_{50} (μ g/mL)	Concentration used (μ g/mL)	$\eta_{C0}:\eta_C(A_1)$	$\eta_{C0}:\eta_C(A_2)$
Str	11.9 (R388 recipient)	0, 10, 20	0.41	0.79
Carb	2.7 (R388 donor)	0, 2, 4	0.90	0.66
Eryth	11.7 (R388 recipient)	0, 10, 20	0.87	0.98
Cm	2.2 (R388 recipient)	0, 2, 4	0.90	0.64
Nor	0.07 (R388 donor)	0, 0.05, 0.1	0.97	0.99

Plasmid: R6K

Antibiotic	IC_{50} (μ g/mL)	Concentration used (μ g/mL)	$\eta_{C0}:\eta_C(A_1)$	$\eta_{C0}:\eta_C(A_2)$
Str	1.88 (R6K recipient)	0, 2, 4	0.82	0.90
Carb	14.8 (R6K recipient)	0, 10, 20	0.76	0.16
Eryth	34.4 (R6K recipient)	0, 30, 60	1.00	1.00
Cm	1.9 (R6K donor)	0, 2, 4	1.00	1.00
Nor	0.07 (R6K recipient)	0, 0.05, 0.1	0.97	0.81

Plasmid: pESBL-283

Antibiotic	IC_{50} (μ g/mL)	Concentration used (μ g/mL)	$\eta_{C0}:\eta_C(A_1)$	$\eta_{C0}:\eta_C(A_2)$
Str	1.88 (R^F)	0, 2, 4	0.80	0.44
Carb	14.8 (R^F)	0, 10, 20	0.91	0.95
Eryth	34.4 (R^F)	0, 30, 60	0.99	1.00
Cm	1.9 (R^F)	0, 2, 4	0.98	1.00
Nor	0.05 (R^F)	0, 0.05, 0.1	0.99	0.99

ESBL #41

Antibiotic	Concentration used (μ g/mL)	$\eta_{C0}:\eta_C(A_1)$	$\eta_{C0}:\eta_C(A_2)$
Str	0, 2, 4	0.76	0.95
Carb	0, 2, 4	0.86	0.87
Eryth	0, 19.2, 38.4	1.00	1.00
Cm	0, 2, 4	0.96	1.00

Nor	0, 0.05, 0.1	1.00	0.75

ESBL #146

Antibiotic	**Concentration used (μ g/mL)**	$\eta_{C0}:\eta_C(A_1)$	$\eta_{C0}:\eta_C(A_2)$
Str	0, 2, 4	0.87	0.18
Carb	0, 2, 4	0.90	0.97
Eryth	0, 19.2, 38.4	0.96	1.00
Cm	0, 2, 4	1.00	1.00
Nor	0, 0.05, 0.1	0.97	1.00

ESBL #168

Antibiotic	**Concentration used (μ g/mL)**	$\eta_{C0}:\eta_C(A_1)$	$\eta_{C0}:\eta_C(A_2)$
Str	0, 2, 4	0.28	0.64
Carb	0, 2, 4	0.67	0.76
Eryth	0, 19.2, 38.4	0.95	0.37
Cm	0, 2, 4	0.40	0.57
Nor	0, 0.05, 0.1	0.14	0.46

ESBL #193

Antibiotic	**Concentration used (μ g/mL)**	$\eta_{C0}:\eta_C(A_1)$	$\eta_{C0}:\eta_C(A_2)$
Str	0, 2, 4	0.49	0.70
Carb	0, 2, 4	0.31	0.66
Eryth	0, 19.2, 38.4	0.92	1.00
Cm	0, 2, 4	0.60	0.83
Nor	0, 0.05, 0.1	0.38	0.48

R^+ donor with ESBL-producing *Klebsiella pneumoniae* recipients

Isolate	**Strep used (μ g/mL)**	$\eta_{C0}:\eta_C(A_1)$	$\eta_{C0}:\eta_C(A_2)$
#109	0,2,4	0.99	0.24
#135	0,2,4	0.81	0.70

Table S4: Dimensional modeling growth equations and parameters

(a) Experimental estimates of growth parameters using plate reader measurements. Each population was screened against Kan and Cm. Populations that were resistant to the antibiotic were fitted with a linear line, while those that were sensitive were fitted using a Hill equation (Methods section Eq. 4).

Population	Antibiotic/experiment	Equation	Experimental fit
R	Cm (Fig. S6b and d)	$\mu_R = \mu_{R_{max}} - m_{R_{Cm}} A$	$m_{R_{Cm}} = 2.17\times10^{-4}$ $\mu_{R_{max}} = 0.32$
R	Kan(Fig. 3d ii-iv)	$\mu_R = \frac{(\mu_{R_{max}} K_R^{n_R})}{K_R^{n_R} + A^{n_R}}$	$\mu_{R_{max}}$=0.28 K_R=2.01 n_R=6.45
R^K	Kan, (Fig. 3d i)	$\mu_{R^k} = \mu_{R^k_{max}} - m_{R^k} A$	$m_{R^k} = 1.38\times10^{-4}$ $\mu_{R^k_{max}} = 0.23$
G	Kan (Fig. 3d i-ii)	$\mu_G = \mu_{G_{max}} - m_G A$	$m_G = 1.86\times10^{-5}$ $\mu_{G_{max}} = 0.33$
G	Kan+4μg/ml Cm (Fig. 3d iii)	$\mu_G = \mu_{G^c_{max}} - m_{G_{Cm}} A$	$m_{G_{Cm}} = 6.57\times10^{-6}$ $\mu_{G^c_{max}} = 0.15$
G	Cm (Fig. 3d iv, Fig. 6b and d)	$\mu_G = \frac{\mu_{G_{max}} K_G^{n_G}}{K_G^{n_G} + A^{n_G}}$	$\mu_{G_{max}}$=0.33 K_G=1.92 n_G=2.19
Y	Kan (Fig. 3d i-iii)	$\mu_Y = \mu_{Y_{max}} + m_{Y_K} A$	$m_{Y_K} = 2.66\times10^{-5}$ $\mu_{Y_{max}} = 0.31$
Y	Cm (Fig. 3d iv)	$\mu_Y = \mu_{Y_{max}} - m_{Y_C} A$	$m_{Y_C} = 2.31\times10^{-4}$ $\mu_{Y_{max}} = 0.31$
B	Cm (Fig. S6d)	$\mu_B = \frac{\mu_{B_{max}} K_B^{n_B}}{K_B^{n_B} + A^{n_B}}$	$\mu_{B_{max}}$=0.25 K_B=1.66 n_B=1.56

(b) Modeling parameters. Parameters were largely chosen based on the values obtained from experimental results in (a). Slopes of all lines were significantly smaller in magnitude than the μ_{max}, and were disregarded. Since the microfluidic environment likely results in slightly different kinetic parameters, the rates and sensitivities were slightly modified to illustrate the generality of every trend. For qualitatively demonstrating results, we assume μ_{max} for the resistant population to be slightly larger than that of the sensitive one. For simulations when we switch the antibiotic (e.g. Cm instead of Kan in Fig. S6a), parameters for $\mu_{r_{max}}$ and $\mu_{g_{max}}$ were switched as well.

Dimensional parameter	Value
$\mu_{R_{max}}$(hr^{-1})	0.25
K_R(μg)	1.6
n_R	7
$\mu_{G_{max}}$(hr $^{-1}$)	0.32
$\mu_{G_{max_{Cm}}}$(hr $^{-1}$)	0.17
K_G(μg)	2.5
n_G	2
$\mu_{B_{max}}$(hr^{-1})	0.2
K_B(μg)	2

n_B	4
$\mu_{Y_{max}}$ (hr^{-1})	0.267
$\eta_C \left(\frac{mL}{Cells \times hr}\right)$	1×10^{-11}
$N_m \left(\frac{cells}{mL}\right)$	1×10^{9}
$R_0\left(\frac{cells}{mL}\right)$	1×10^{6}
$G_0\left(\frac{cells}{mL}\right)$	1×10^{6}
A (μg)	[0.5 5]
t (hr^{-1})	[0 60]

(c) Nondimensional variables, parameters, and values used for simulations.

Nondimensional variables and parameters	**Value**
$g = \frac{G}{N_m}$	$g_0=1\times10^{-3}$
$r = \frac{R}{N_m}$	$r_0=1\times10^{-3}$
$y = \frac{Y}{N_m}$	$y_0=1\times10^{-3}$
$a = \frac{A}{K_R}$	[0.03, 3.1]
$\tau = t\mu_{Y_{max}}$	16
$\mu_{g_{max}} = \frac{\mu_{G_{max}}}{\mu_{Y_{max}}}$	1.20
$\mu_{g_{max_{Cm}}} = \frac{\mu_{G_{max_{Cm}}}}{\mu_{Y_{max}}}$	0.64
$\sigma_g = \frac{K_G}{K_R}$	1.56
$\sigma_b = \frac{K_B}{K_R}$	1.25
$\eta_C^{'} = \frac{\eta_C N_m}{\mu_{Y_{max}}}$	0.0375
n_r	7
n_g	2
n_b	4

Table S5. Summary of experimental conditions

(a) A brief description of the strains and antibiotics used for each microfluidic experiment. All experiments here are included in Fig. 4 power law correlation.

Experiment	**1 (Fig. 3d i)**	**2 (Fig. 3d ii)**	**3 (Fig. 3d iii)**	**4 (Fig. 3d iv)**	**5 (Fig. S6b left)**	**6 (Fig. S6b right)**	**7 (Fig. S6d)**
General description	Both G and R resistant to [A]	Only R is sensitive to [A], but growth rates never intersect	Only R is sensitive to [A], but growth rates do intersect	Both G and R sensitive to [A]	Using Cm instead of Kan	Same as 5, but switching the direction of transfer	Same as 5, with the addition of a buffer population
Color	Red	Blue	Pink	Gray	Green	Yellow	Purple
Donor (resistance)	G^+, (kan^R)	G^+, (kan^R)	G^+, (kan^R)	G^+, (kan^R)	G^+, (kan^R)	R^+, (cm^R)	G^+, (kan^R)
Recipient (resistance)	R^k, (kan^R)	R^- (cm^R)	R^- (cm^R)	R^- (cm^R)	R^- (cm^R)	G^- (kan^R)	R^- (cm^R)
Kan (μg/ml)	0, 2, 4, 8, 25	0,1,2,4,6,10,50	0,1,2,4,6,10	0,1,2,4,6,10	0	0	0
Cm (μg/ml)	0	0	4	0,1,2,4,6,10	0,1,2,4,10,50	0,2,4,8,10,50	0,1,2,4,8,50

(b) A summary of processing for experiments in Figure 3d i-iv, including the total number of chambers collected, the number of chambers removed through the outlier process, and the date the experiment was performed on.

Fig. 3d i.

Concentration (Kan, Cm)	(0,0)	(2,0)	(4,0)	(8,0)	(25,0)	(50,0)
Total number of chambers collected	10	10	10	10	10	10
Chambers removed	1	2	0	0	1	1
Experiment date	01282015	01282015	01282015	01282015	01282015	01282015

Fig. 3d ii.

Concentration (Kan, Cm)	(0,0)	(1,0)	(2,0)	(4,0)	(6,0)	(10,0)	(50,0)
Total number of chambers collected	10	8	8	8	8	8	10
Chambers removed	1	2	0	3	1	1	1
Experiment date	01062015	02062015	02062015	02062015	02062015	02062015	12152014

Fig. 3d iii.

Concentration (Kan, Cm)	(0,4)	(1,4)	(2,4)	(4,4)	(6,4)	(10,4)

Total number of chambers collected	10	10	10	10	10	10
Total number of chambers removed	1	1	1	1	0	1
Experiment date	01242015	01242015	01242015	01242015	01242015	01242015

Fig. 3d iv.

Concentration (Kan, Cm)	(0,0)	(1,1)	(2,2)	(4,4)	(6,6)	(10,10)
Total number of chambers collected	10	10	10	10	10	10
Chambers removed	3	0	1	1	1	1
Experiment date	09092015	09092015	09092015	01242015	05292015	05292015

Fig. S6b left panel

Concentration (Kan, Cm)	(0,0)	(0,1)	(0,2)	(0,4)	(0,10)	(0,50)
Total number of chambers collected	10	10	10	10	10	10
Chambers removed	0	1	1	0	1	1
Experiment date	06182015	06182015	06182015	06182015	06182015	06182015

Fig. S6b right panel

Concentration (Kan, Cm)	(0,0)	(0,2)	(0,4)	(0,8)	(0,10)	(0,50)
Total number of chambers collected	10	10	10	10	10	10
Chambers removed	1	1	2	1	0	1
Experiment date	05142015	05142015	05142015	05142015	05142015	05182015

Fig. S6d

Concentration (Kan, Cm)	(0,0)	(0,1)	(0,2)	(0,4)	(0,8)	(0,50)
Total number of chambers collected	10	10	10	10	10	10
Chambers removed	2	2	0	1	2	2
Experiment date	06112015	06112015	06112015	06112015	06112015	06112015

Video S1: Control experiment for *oriT* specificity. G^+ and R^- cells mixed together and pre-grown in the chamber for four hours in M9 media with IPTG (1 mM) and Tet (20 μg/ml). After pre-incubation, media was switched to that containing selecting concentrations of Kan (50 μ g/mL) and Cm (100 μ g/mL). Cells that contain resistance to both antibiotics, the transconjugants, grow, indicating the ability for *oriT* to transfer the GFP plasmid. These appear yellow by eye, due to the overlap from GFP and mCherry. Time-lapse images are obtained every 5 minutes for 27 hours. Video is arbitrarily contrast adjusted to demonstrate dynamics for visual purposes only. Raw videos were used for data analysis.

Video S2: Control experiment for *oriT* specificity. G^- (not containing *oriT*) and R (no *oriT*) cells mixed together and pre-grown in the chamber for four hours in the same conditions as Video S1. Once the media was switched to that containing antibiotic, no cells are able to proliferate, indicating that the mobilizable plasmid expressing GFP is only transferrable if it contains the *oriT* sequence. GFP-expressing cells remain in the chamber after the experiment since Cm is bactericidal, and thus will inhibit growth but not induce lysis. Video is arbitrarily contrast adjusted to demonstrate dynamics for visual purposes only. Raw videos were used for data analysis.

References

1. Gullberg, E. *et al.* Selection of resistant bacteria at very low antibiotic concentrations. *PLoS Pathog* **7,** e1002158 (2011).
2. Händel, N., Otte, S., Jonker, M., Brul, S. & ter Kuile, B. H. Factors that affect transfer of the IncI1 β-Lactam resistance plasmid pESBL-283 between *E. coli* strains. *PLoS ONE* **10,** (2015).